THE EFFECT OF ELEVATED WATER CONTENT ON SWIRL-STABILIZED ETHANOL/AIR FLAMES

Baine B. Breaux and Sumanta Acharya
Louisiana State University
Turbine Innovation and Energy Research Laboratory
Baton Rouge, Louisiana, USA

ABSTRACT

Ethanol is currently being considered as a potential alternative to traditional fuels. This study seeks to validate the use of hydrous ethanol in lieu of fossil fuels or anhydrous ethanol in order to reduce the production cost associated with ethanol. Experiments are conducted in a swirl-stabilized combustor, representative of a gas turbine and hydrous ethanol ranging from 0%-40% water by volume are tested. A stable flame was achieved for fuels up to 35% water and the lean blow out limit was determined for these fuels. Fuels ranging from 0% to 20% water were tested in greater detail which included thermal mapping of the flame, exhaust temperature measurements, exhaust NO_x, CO_2, and O_2 measurement, as well as CH* and OH* imaging of the flame. Equivalence ratio within the combustor was varied to include 0.6, 0.8, 1.0 and 1.1, representing extremely lean, lean, stoichiometric, and rich test conditions, respectively. Results revealed that the exhaust heat rate, combustion efficiency, and combustor thermal efficiency were not affected negatively by elevated water content up to 20%. However, the flame temperature did generally decrease as a result of water addition, particularly in the lower flame region. CH*/OH* emissions in the lower-flame region were also appreciably reduced due to the parasitic heat load of water vaporization and local quenching in the lower parts of the flame. The practical consequence of burning hydrous fuel was reduced exhaust temperature. Reduced peak temperatures lead to reductions of exhaust NO_x at all test conditions. This study indicates that hydrous ethanol with up to 20% water can potentially be used in lieu of the more expensive anhydrous ethanol for combustion applications.

Keywords: Ethanol, Hydrous, Combustion, Swirl-Stabilized

Abbreviations: LBO: Lean Blow Out; ER: Equivalence Ratio; GC: Gas Chromatograph; IC: Internal Combustion; ICCD: Intensified Charge Coupled Device; NASA: National Aeronautics and Space Administration; CEA: Chemical Equilibrium with Classifications; DAQ: Data Acquisition System; UV: Ultra Violet; LHV: Lower Heating Value; NPT: National Pipe Thread

Corresponding Author: ___Dr. Acharya please include permanent address, phone number, and desired email here___

1. Introduction

As global demand for hydrocarbon fuel continues to rise and available reserves of fossil fuels decrease, significant attention is being given to the development of renewable hydrocarbon fuel sources. This includes the development of bio-alcohol fuels such as ethanol. A number of studies have been performed to evaluate the feasibility of ethanol as an alternative fuel for operating internal combustion (IC) engines [1, 2, 3]. More recently, the viability of bio-fuels, including ethanol, has been explored in turbine engines both for power generation and aircraft propulsion [4]. Ethanol can replace light distillates such as gasoline and some middle distillates such as kerosene without significant changes to existing equipment or infrastructure. Blends of ethanol and conventional fuels have also been tested and have shown some promise as potential fuels [5].

The most well-known drawback of ethanol as a fuel is its relatively low heating value when compared to traditional hydrocarbon fuels. The Lower Heating Value (LHV) of pure ethanol is 21.3 MJ/L compared to a LHV of 34.9 MJ/L for Jet A fuel and 33 MJ/L for gasoline [1, 4]. Therefore, in order to be competitive in terms of price per unit of energy delivered production costs for ethanol need to be substantially lower than those of standard hydrocarbon fuel. This is currently not the case because water removal is a significant cost in anhydrous ethanol production. Two approaches that are being investigated for addressing the energy/cost issue are either to boost the volumetric energy density of the fuel through the use of energetic fuel additives [6, 7] or to explore the use of hydrous ethanol so that production costs are minimized. The latter approach is explored here.

The ethanol production process includes distillation and more complicated methods such as molecular sieves to remove water from the fuel. At ethanol concentrations greater than 95.57% ethanol, or 192 proof (E95.5/W4.5), hydrous ethanol is an azeotropic mixture. Because of the azeotropic nature of this mixture a significant additional investment in energy and capital is required to achieve anhydrous fuel [3]. Additional economic gains can be achieved from reduced distillation costs if the final ethanol concentration is below the azeotropic limit [8]. These gains will potentially be greater than the losses resulting from increased transportation costs [9]. It has been claimed that the production and efficient use of 70 proof ethanol (E35/W65) would result in a 34% increase in the net energy gain when compared to anhydrous ethanol [2] due to the reduction in the water separation cost from 37% of the total production cost for anhydrous ethanol down to 3% of the total production cost while producing E35/W65 [2]. The use of 70 proof ethanol, which is 65% water by volume, is an unlikely candidate for combustion applications because of reduced temperatures and water-quenching effects. However, it is possible to find a more moderate proof of hydrous ethanol that will result in reasonable functionality while still substantially reducing the cost of ethanol production. For example, the use of an E80/W20 would require approximately a quarter of the distillation energy required to achieve E96/W14 [9].

Lower proof ethanol possesses fewer ethanol molecules per unit volume than pure ethanol because ethanol molecules are displaced by an increasing amount of water. Correspondingly, the LHV, both on a volumetric and gravimetric basis, of the fuel is reduced with increasing water content. Therefore the use of a lower-proof ethanol fuel results in the consumption of larger volumes of fuel to produce the same amount of energy, but may be economically advantageous.

Previous studies have considered the use of wet ethanol in IC engines [2, 3, 10] or have considered the burning velocity of hydrous ethanol at concentrations greater than 170 proof (E85/W15) [11]. Limited work, however, has been done concerning the use of wet ethanol in a swirl-stabilized continuous flame combustor. Information provided from such a study will be particularly relevant to the use of wet ethanol in turbine and industrial burner applications.

It is known that increasing water content of the fuel will decrease the adiabatic flame temperature of the combustion reaction. Adiabatic Flame Temperatures for perfectly mixed reactions were calculated using NASA CEA code [12] for various equivalence ratios and water concentrations and is presented in Figure 1. This reduction in temperature will undoubtedly result in a reduction in NO_x formation by reducing thermal NO_x. This decrease in adiabatic flame temperature is accompanied by an increase in latent heat of vaporization. Water requires more heat to evaporate than ethanol and as a result the amount

of heat required to vaporize a high water content fuel is greater. These characteristics of hydrous ethanol may have adverse effects on fuel vaporization and combustion efficiency. The operational limits of the combustor, in terms of Equivalence Ratio (ER), may be affected adversely by low alcohol proof.

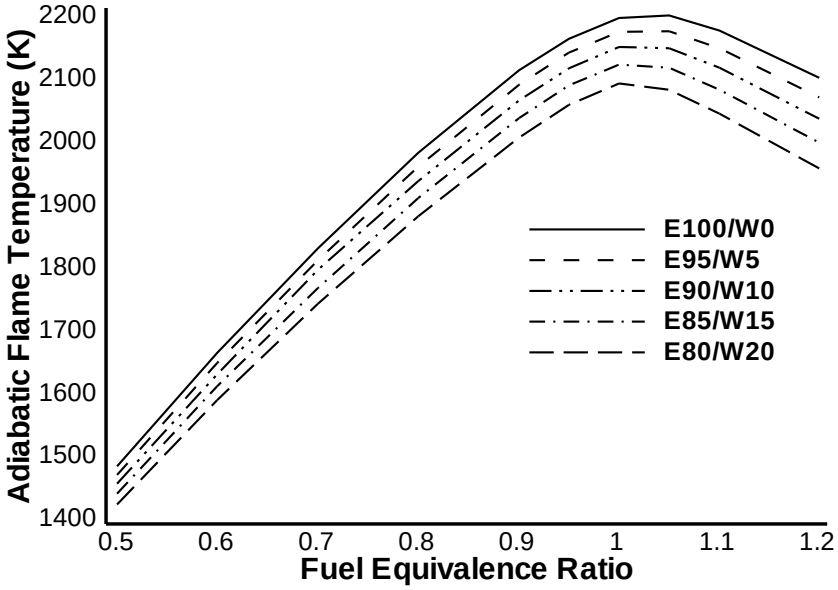

Figure 1: Adiabatic Flame Temperature of Hydrous Ethanol, Calculated Using NASA CEA Code [12]

This paper seeks to provide a detailed view of how increasing water content effects flame structure, flame stability, flame temperature, heat release, and exhaust NO_x, CO_2, and O_2 concentration. Two studies using this experimental apparatus have been presented previously. The first paper focused on flame temperature and LBO measurements [13] while the second paper focused on chemiluminescence diagnostics [14]. This study is unique in combining the results from previous studies, along with additional exhaust gas measurements, to make complex conclusions. This study represents the only comprehensive study of a hydrous ethanol flame in a swirl-stabilized combustor. It is pertinent to understand how elevated water content affects the operational limits and performance of the swirl-stabilized combustor. This information is particularly relevant in evaluating hydrous fuel as a candidate in fuel flexible gas turbine operation or fuel flexible industrial burners.

2. Materials and Method

2.1 Experimental Setup

The experimental setup, shown in Figure 2, uses a vertically oriented swirl-stabilized combustor that is circular in cross section. The combustor exit is unrestricted, allowing for atmospheric pressure, and the inlet is a dump diffuser with an area ratio of 35.73. The combustor shell inside diameter is 27.3 cm with a single fuel atomizer located at the center of the dump plane. For all experiments the air flow rate was held constant at 18.88 L/s. This ensures that the air flow velocity field within the combustor does not vary between tests. Axial vane swirlers were utilized in conjunction with the dump to stabilize the flame and induce hot gas recirculation. Two swirlers are situated at locations 2.54 and 19.05 cm upstream of the dump plane. Each of these swirlers has eight 45° vanes, resulting in a geometric swirl number of 0.755. Absolute air velocity as it exits the swirler is calculated as 22.3 m/s, with tangential and axial components both equal to 15.8 m/s. Turbulence intensity of the non-reacting air flow was measured using an IFA-300 hot-wire anemometer system, revealing a minimum turbulence intensity of 25% at all radial locations for axial locations closer to the dump plane than x/D=0.60.

Fuel is supplied to the center of the combustor through a lone single-point Parker-Hannifin pressure swirl atomizer with a hollow cone spray pattern. The nozzle tip is situated 1.27 cm below the dump plane. This location was chosen to enhance flame anchoring through the use of swirl and provide a more consistent flame structure. The tests span a wide range of fuel flow rates, varying from 0.123 to 0.282 L/min. This is necessary to achieve the wide range of equivalence ratios desired with each fuel composition. In order to achieve this range of fuel flow rates nozzles were interchanged throughout the study. All nozzles follow the same design but are scaled up to accommodate the varying fuel flow rate. Nozzles used include nominal ratings of 0.126, 0.158, 0.189 and 0.221 L/min at 689.47 kPa. These nozzles are going to be referred to as nozzles A, B, C, and D, respectively. Fuel supply pressure varies from 517 to 123 kPa which results in droplet sizes that are estimated, based upon manufacturer's performance curves, to be consistently between 17.5 and 27.5 microns (Sauter Mean Diameter).

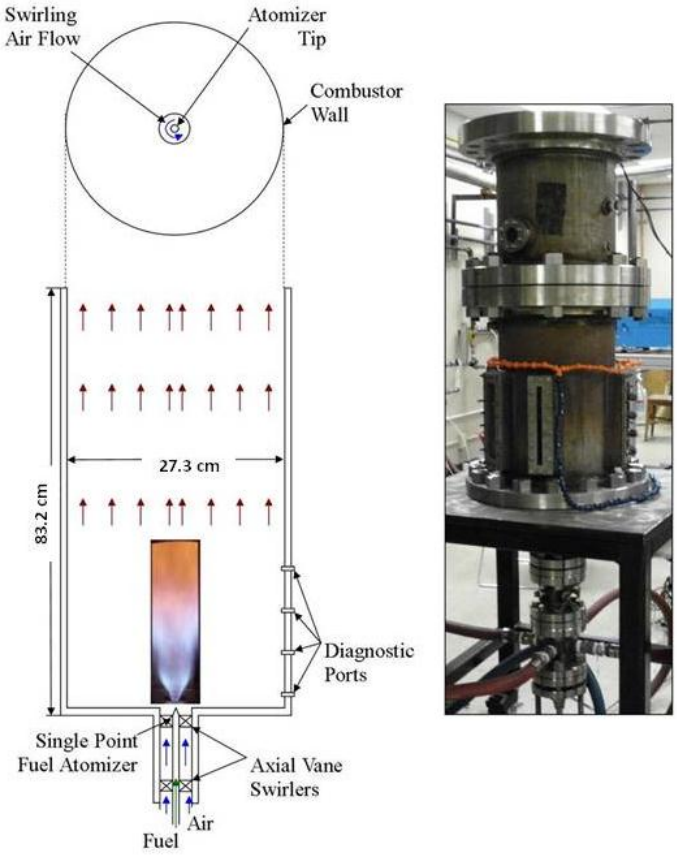

Figure 2: Test Apparatus

The flame and hot gas stream can be accessed through a series of 0.5 inch NPT (1.27 cm) ports, at locations 1.27, 3.81, 6.35, 8.89, 11.43, 13.89, 15.24, 35.56, 45.72, 50.80, 55.88, 60.96, and 63.5 cm above the dump plane as well as at the combustor exit 0.84 meters downstream of the dump. It is through these ports that temperature measurements are taken utilizing a Type B thermocouple rake manufactured by Gulf Sensors, Inc. The rake has thermocouples capable of taking five temperature measurements at 2.54 cm intervals in the radial direction, starting at the flame centerline and moving towards the combustor wall. Exhaust temperature measurements are taken using a similar rake located at the combustor exit. The temperature readings were subjected to cold-junction compensation methods employed by the National Instruments 9211 DAQ module.

The combustor allows for optical access via a 6.35 x 20.32 cm UV grade fused silica window, thickness 1.27 cm. Flame images were taken through this window using a Photron Fastcam SA3 camera.

This high speed, high resolution camera is capable of resolving 2000 frames per second at a resolution of 1024x1024 pixels. This camera was used in conjunction with an UVi Invisible Vision intensifier, model 1850-10, in order to extend the spectral range of the setup to enhance the sensitivity within the images in the low UV range while providing a fast-gating option that will enable high speed images. The camera was set up at a focal length of approximately 1.37 m from the combustor center plane. This results in a field of view 7.2 cm x 18.6 cm at the combustor center plane and a resolution 3025 pixels per cm^2 (55 pixels per cm). The modular design of the combustor also allows for an alternative configuration that permits the same quality of image to be generated at a cross section 0.40 to 0.59 meters downstream of the dump plane.

Optical and chemiluminescence methods are utilized to resolve time and spatially dependent heat release. This is done through the use of CH*and OH* imaging. It is generally accepted that CH* and OH* are indicators of the reaction zone. CH* can be taken as an indicator of the onset of combustion [15] and OH* is primarily formed through CH* oxidation and indicates a later phase of combustion [16]. Though some criticism of the technique has been intermittently discussed [17] this criticism generally applies to CH* emissions from premixed flames. Previous studies with continuous ethanol flames have taken the presence of CH* to indicate global heat release distribution [6, 17] and the temperature has even been accurately predicted using CH* as an indicator [18]. Narrow band interference filters are utilized to determine the spatial distribution of CH* and OH*. OH* is captured using a 50 mm diameter, 307 nm +/- 2 nm, FWHM=10nm. CH* is captured using a 50 mm diameter, 430 nm +/- 2 nm, FWHM=10nm. These wavelengths have been used to represent CH* and OH* in various past works [6, 17, 19].

NO_x measurements are taken from gas sampled from the centerline at the exit of the combustor. This is taken using a Cambustion fNOx 400 system which reads the concentration of NO_x in the hot gas stream with a frequency of 250 Hz. This device allows NO_x to react with Ozone at elevated temperature and determines NO_x ppm by monitoring the strength of the chemiluminescent signal from the reaction.

O_2 and CO_2 measurements were also taken from the centerline at the combustor exit. These measurements were made using an Agilent 490 micro gas chromatograph. This device separates gases by thermal conductivity and uses EZ-Chrome SI software to analyze the results based upon a stored calibration. O_2 was resolved using a MS5A column while CO_2 was resolved using a PPU column. The sample line was heated to prevent contamination by condensate and calibration gas was re-analyzed after each set of data to verify accurate analysis. Sample time was set to 2 minutes in order to ensure complete purging of the sample line for each measurement.

The combustor was ignited using a retractable assembly equipped with a Woodward Governor igniter. This 15 kV igniter was capable of delivering 1.5 J per spark. This device was capable of igniting all fuels tested in this study from multiple locations within the combustor.

2.2 Test Conditions

In this study ethanol with various water concentrations were tested. Fuel composition will be denoted in the following form: EXX/WYY where E stands for Ethanol, W for Water, and XX and YY represent the volumetric percentages of ethanol and water, respectively. For example, E100/W0 represents 100% ethanol and 0% water or 200 proof ethanol, while E75/W25 represents 75% ethanol and 25% water or 150 proof ethanol. The fuels tested were E100/W0, E95/W5, E90/W10, E85/W15, E80/W20, E75/W25, E70/W30, E65/W35 and E60/W40. Fuel was premixed at a temperature of 297.4 K using eye measurements and standard beaker mixing techniques. Both air and fuel are injected into the combustor at 297.4 K. Air flow rate is held constant while fuel flow rate is altered to achieve the target equivalence ratios of 0.6 (lean), 0.8, 1.0 (stoichiometric) and 1.1 (rich). As the water content is increased the lean conditions became less stable and in some cases were unachievable. The test conditions that were realized and the corresponding nozzle selections are tabulated in Table 1. Evaluating both air and fuel supply systems and performing an uncertainty analysis for the equivalence ratio calculation reveals that the uncertainty of the ER is less than 5.25% for all equivalence ratios. This equates to a maximum ER error of 0.0315 at ER=0.6 and error of 0.0577 at ER=1.1.

The nozzle choices were dictated by practical considerations. Nozzle 'A' could not be used to achieve all equivalence ratios because the required increase in fuel supply pressure would result in significant changes in spray pattern and atomization quality. Nozzle 'C' could not be used for the lower flow rate conditions because fuel pressure was too low and atomization became exceptionally poor, resulting in an under-developed spray cone. The nozzle selection seeks to minimize these affects and provide rough comparability in spray patterns and drop sizes between different fuel compositions for a given equivalence ratio. This was done with the aid of manufacturer-supplied performance data for the atomization nozzles as well as through an extensive flame and spray structure tuning process.

A stable flame could not be achieved at water concentrations greater than E65/W35, regardless of equivalence ratio. Furthermore, the full range of fuel compositions was not tested for some measurements. This is because initial tests demonstrated a limited operating range for fuels with water content greater than E75/W25. Deeming these fuels impractical because of the narrow range of operability, and in the interest of time, the fuel composition was restricted to less than 20% water for later measurements.

Table 1: Test Conditions and Nozzle Selection

Fuel Composition	Equivalence Ratio			
	0.6	0.8	1.0	1.1
E100/W0	A	A	C	C
E95/W5	A	A	C	C
E90/W10	A	A	C	C
E85/W15	A	A	C	C
E80/W20		B	C	C
E75/W25		B	C	C
E70/W30			C	C
E65/W35			D	D

Table 2: Parker Hannifin Single-Point Hollow Cone Nozzle Specifications

Nozzle	Nominal Flow Rate (L/min Water at 689.37 kPa)
A	0.126
B	0.158
C	0.189
D	0.221

3. Results and Discussion

3.1 Lean Blow Out

In many cases it is pertinent to know the lower limit of equivalence ratio at which a stable flame can be achieved for a given fuel. This is particularly relevant in industrial gas turbine or burner applications where engines are frequently run near their lean limit to conserve fuel and control emissions. The lower limit of equivalence ratio is referred to as the Lean Blow Out (LBO) limit. The equivalence ratio is calculated based on the ethanol to air ratio. The volumetric content of the water is not included in the calculation.

The LBO of the flame was evaluated as fuel water content varied, resulting in a relationship between the water content and the minimum ER that is achievable (Figure 3). Nozzle selection was determined by utilizing the smallest nozzle capable of achieving a stable flame at one of the established test conditions of ER=0.6, 0.8, 1.0, or 1.1. The use of a larger nozzle shifts the LBO trend upward. This is because using a larger nozzle results in low fuel pressure at a low ER, this in turn results in poor atomization of the fuel and poor flame quality. Repeatability error bars are shown and indicate high repeatability over three runs. It can also be seen that with some fuels (E100/W0, E95/W5 and E90/W10) the LBO ER is below the theoretical limit of 0.5 [20]. This is because, while global ER will theoretically not allow for a stable

flame, the current configuration is non-premixed and downstream local mixing effects result in a local ER that is within the acceptable range for achieving a flame.

From this data it is clear that in general the LBO limit increases as water content increases. The water acts as a heat sink in the vaporizing fuel and as the water content is elevated the volume flow rate of fuel must increase to maintain the same equivalence ratio. Due to the increased flow of water the heat required to vaporize the fuel increases since water absorbs some of the heat of combustion. Therefore more fuel, and consequently a higher equivalence ratio, is required to meet the demand for water vaporizing heat. Despite this negative consequence of water addition it is pertinent to note that LBO is still acceptably low (ER<0.6) for all fuels with less than approximately 27% water.

It is interesting to note that LBO decreases when fuel composition changes from E100/W0 to E95/W5. This indicates that the addition of water to the fuel in low levels may actually decrease the LBO limit and stabilize the flame. This opposes the general LBO-Water Content relationship. It is hypothesized that the addition of water in low levels acts to stabilize the flame by reducing flame propagation velocity. This would delay the burning rate and prevent local extinction caused by fuel starvation in fuel lean regions. It also may be possible that the addition of water simply leads to increases in the amount of hot vapor in the reaction zones, resulting in a more uniform temperature distribution and increased stability. High speed analysis of the LBO phenomenon is necessary to validate these hypotheses and is not included in this paper.

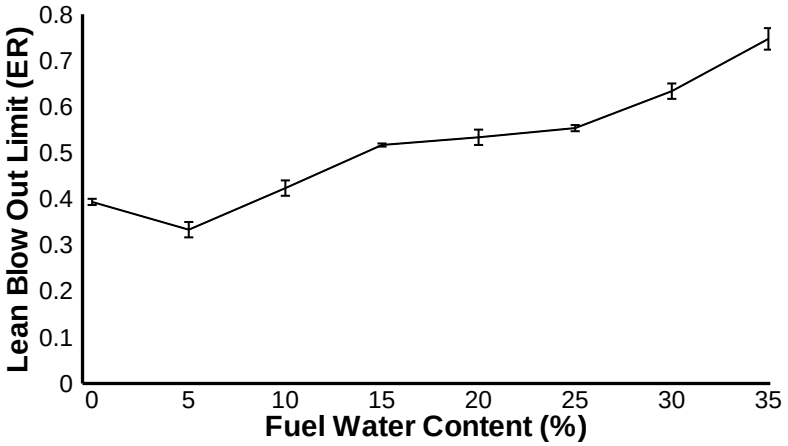

Figure 3: LBO Dependence Upon Fuel Composition

3.2 Flame Temperature

Temperature maps were generated within the base of the flame for different water concentrations. This was done by recording the flame temperature at 24 different locations in a plane through the flame centerline. The resulting 12.7 cm by 15.24 cm image ($0.047 \leq x/D \leq 0.698$; $0 \leq r/D \leq 0.51$) was then mirrored across the flame centerline to give an accurate temperature map of the flame base. This allows for visualization of flame 'hot zones' as they vary with not only the fuel composition but also the equivalence ratio. Each data point depicted is representative of the average temperature at that location, determined after two runs. These temperature contour plots are shown in Figure 4. The flame centerline is represented on the R-axis at location r/D=0. The color-bar indicates a color scale ranging from 400 to 1500 K. This scaling and dimensioning is consistent for all temperature contour plots shown in this paper. Test condition E95/W5, ER=0.6, was analyzed in greater detail, recording flame temperature at 96 locations for a more detailed contour. The maximum percentage difference between the two levels of resolution is on the order of 10% variation, thus validating the use of 24 location flame maps as a time effective way to approximate temperature distribution. Thermocouple measurements are accurate to +/- 0.5%.

The contour plot developed with E95/W5, ER=0.6 depicts the typical features seen in the contour plots. The extremely cold regions, located near the dump plane at a radial location of approximately r/D=0.15, are caused by the heat sink of fuel vaporization. Recall that fuel is injected in a hollow cone at radial location r/D=0 at an axial location x/D=0.047 below the bottom of this plot. The hot region along the flame centerline shows the central hot gas recirculation zone, caused by the swirl stabilization. Similarly, the slightly colder areas near the combustor wall at the dump plane represent areas where dead space occurs in the corner of the combustor. The hot regions located at r/D=0.23 between axial locations of x/D =0.326 and x/D=0.512 represents the hot zone that is expected within and immediately downstream of the primary reaction zone. The large amount of heat released in this primary reaction zone shows up in these hot spots and dissipates as the hot gas moves farther downstream.

Considering temperature behavior as ER and water content vary, it can be seen that for E100/W0 it was found that as ER increases three primary changes occur. First, the temperature generally increases with ER due to the greater fuel content in the feed stream. Second, the reaction 'hot zones' extend farther downstream due to the increase in time taken to fully atomize and vaporize the larger volume of fuel. Third, the shear-layer hot zones are seen to combine with the hot central recirculation zone. This is again attributed to the increased availability of fuel within the flame and the larger width of the shear-layer reaction zones. Similar trends are observed with E95/W5 and E90/W10. When fuel composition is changed to E80/W20 it is found that the combination of the reaction hot zones and the central recirculation zone does not occur until ER=1.0 when it was previously observed at ER=0.8. This is expected because the increased water content scavenges heat from the low flame region.

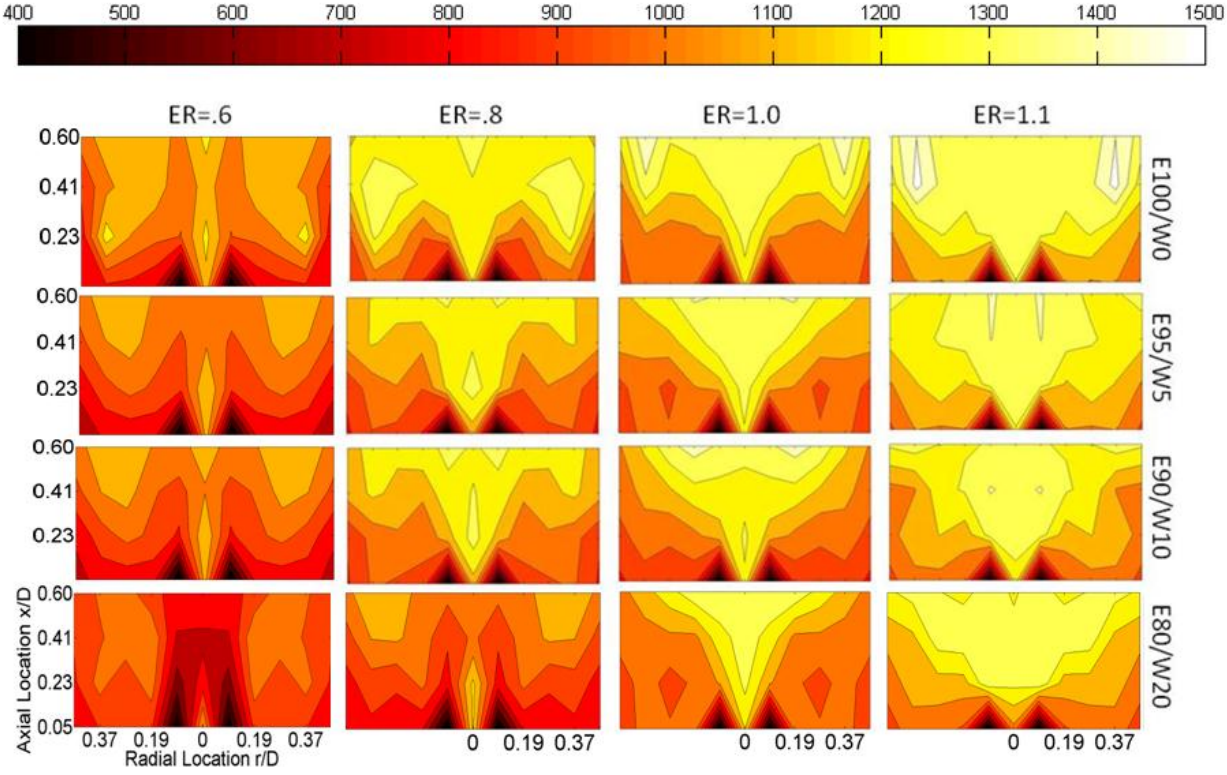

Figure 3: Flame Temperature Contours for Various Fuels and ER

To examine the effect of increasing water content and observing the results at ER=0.8, it is seen that generally temperature reduces as water content increases. It is also seen that the peak temperatures are found farther from the dump plane as water content increases. Again, this is due to the delayed evaporation of the hydrous fuel. Similar trends are observed for all equivalence ratios.

Having established that elevated water content leads to reduced temperature in the low-flame region, and that for higher-water content fuel the combustion zone is relocated farther downstream, it becomes

relevant to evaluate temperature in the latter regions of the flame. This was done by reconfiguring the combustor shell to provide access to a region of the flame farther from the dump plane. Radial temperature profiles were taken at a number of axial locations. Flame temperature contours were generated near the downstream window for a range of water contents at ER=1.0. The contour plots included 24 measurements at axial locations 0.46 to 0.61 meters downstream of the dump plane (1.67<x/D<2.23). These measurements were run-averaged to produce repeatable contour plots. Figure 5 displays both upstream and downstream temperature contours for various fuel compositions at ER=1.0. All dimensions and spacing between the two contours are to geometric scale. The grey block represents the gap between the two measurement planes where access ports to measure temperatures were not available. From these contours it is clear that increasing water content does not drastically change the structure of the temperature contour within the flame, it does however lead to lower temperatures within the combustor.

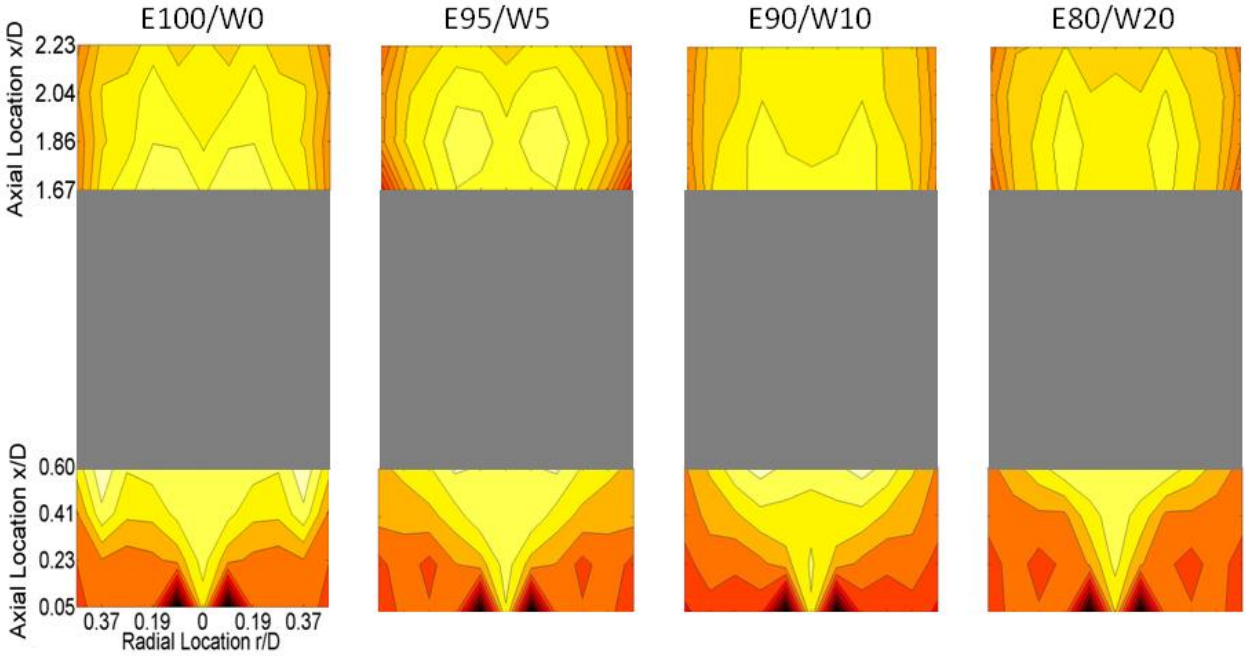

Figure 5: Upstream and Downstream Flame Temperature Maps for Various Fuel Compositions, ER=1.0

Figure 6 shows the temperature distribution along the combustor centerline for both E95/W5 and E80/W20 fuels. Even along the centerline, where temperature differences for different water contents are expected to be the lowest, elevated water content reduces flame temperature, primarily near the dump or combustor base. From Figure 5 and 6 it can be concluded that increasing water content generally reduces flame temperature.

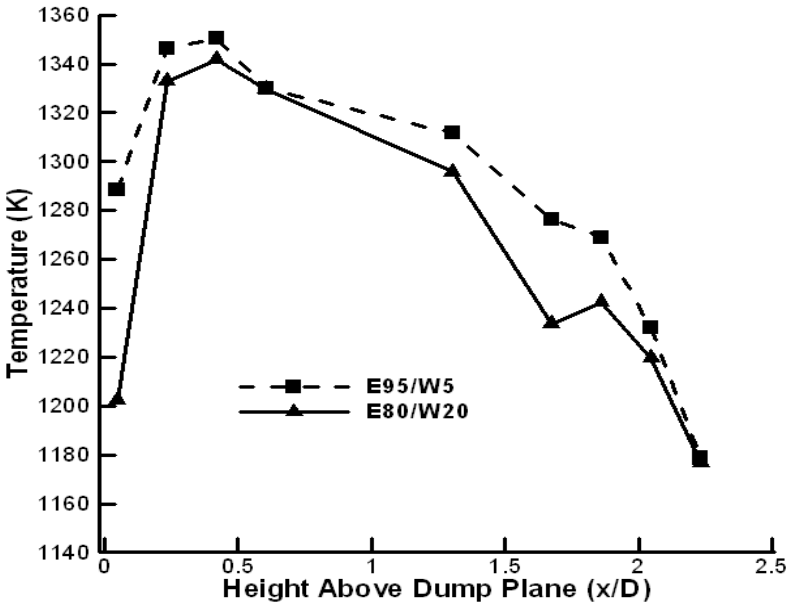

Figure 6: Flame Temperature Measurements at ER=1.0 Along the Combustor Centerline

Figure 7 presents a detailed comparison of radial temperature distribution at different axial locations for E95/W5 and E80/W20 at ER=1.0. At x/D=0.05, the low temperature region near r/D=0.1 corresponds to the unevaporated spray core, but it can be seen that along the centerline the recirculating hot gases lead to elevated temperatures (>1200 K) while along the outer edges of the spray temperatures are in the 1000 K range. By x/D=0.23, the spray has moved radially outwards (r/D>0.2) as represented by the lower temperature region, and has mostly evaporated. Significant combustion of the vaporized fuel occurs in the x/D=0.23-0.60 region as evidenced by the increasing temperatures, with the E95/W5 fuel experiencing earlier combustion (temperatures elevate by x/D=0.42) due to the lower water content, and the E80/W20 showing rapid temperature increases later from x/D=0.42-0.60. In general temperature reduction as well as a more uniform distribution of heat within the combustor is observed with the higher water content, and leads to the reduced concentration of exhaust NO_x presented in this study.

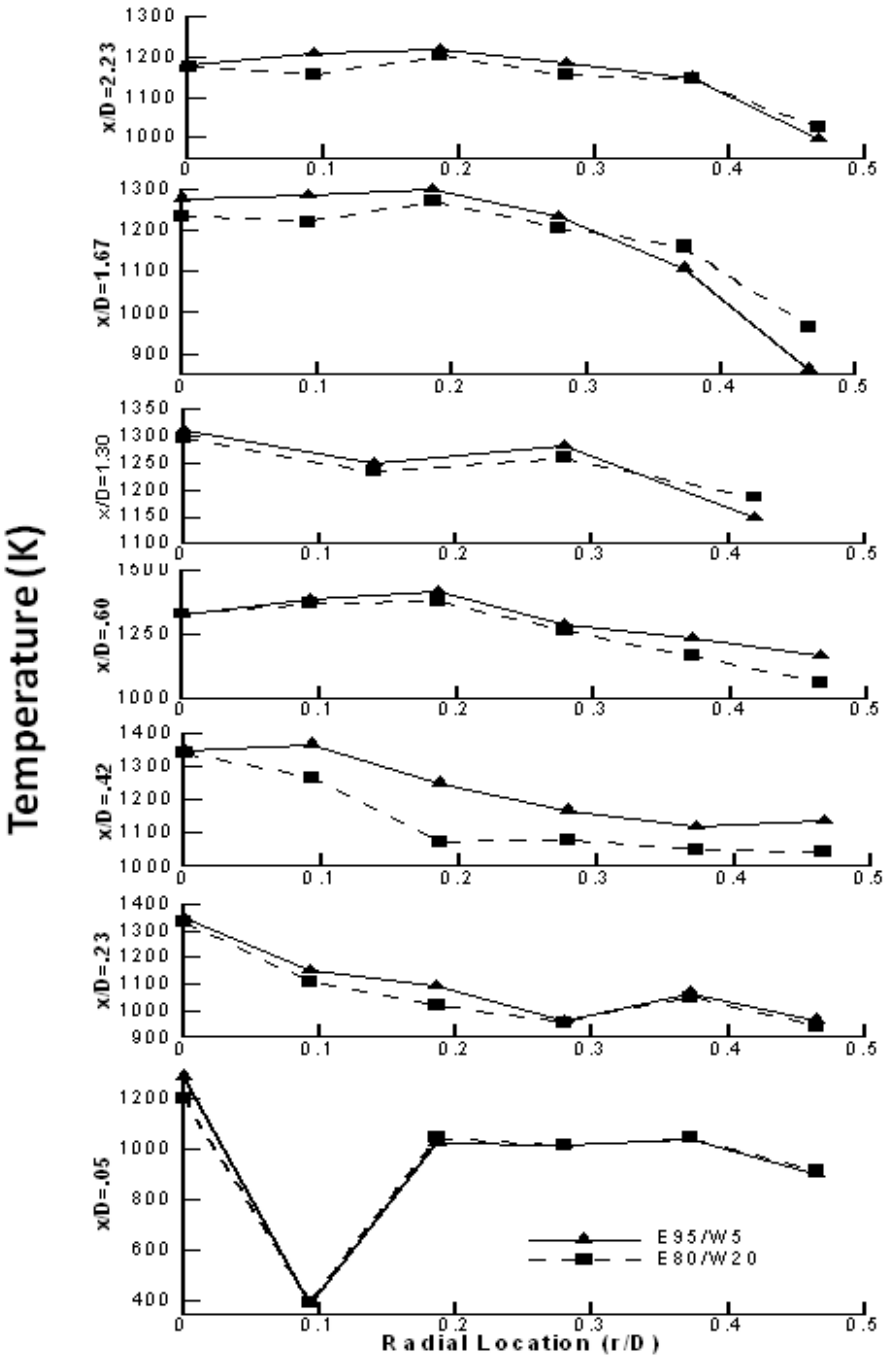

Figure 7: Radial Temperature Distribution at Various Axial Locations, ER=1.0

3.3 Time Averaged Low-Flame CH* Imaging

CH* images were taken at 2000 frames per second for each test condition using a Photron ICCD camera with a gated filter centered at 430 nm. Each image set consist of a total of 500 images collected to cover a total time of 0.25 s, resulting in 0.5 ms between images. UVi intensifier gate time was set to 200μs, F number on the focusing lens was set to 8, and UVi gain was set to 76. This resulted in sensitive capture of CH* chemiluminescence while still offering adequate spatial and time resolution. Three image sets were taken at each test condition and the combustor was allowed to cool between runs.

To qualitatively assess global heat release distribution the CH* image set was averaged with respect to time. Time-averaged images were generated for each image set resulting in three averaged images for each test condition. These time-averaged images exhibited reasonable repeatability [19] and were averaged together to obtain a time-averaged, run-averaged image. Figure 8 shows the results as fuel composition and equivalence ratio vary. The bottom of each image is located 0.5 cm above the combustor dump plane. CH* intensity is indicated by the color bar shown. Color scaling is consistent between all CH* images, units are an arbitrary intensity unit and images offer a qualitative comparison within the CH* set. It is important to note here that the flame front extends out of the field of view. These images represents a line of sight measurement and do not represent the CH* distribution within a flame center plane. From a typical CH* image (e.g. E95/W5) it is possible to see the flame front represented by the primary tulip structure that is stabilized near the injection point and is mostly within the field of view. However, a second region of increased CH* intensity is found between x/D=0.3 and x/D=0.5. Visual inspection of the flame suggests that this second high CH* region is wider than the camera field of view and is subject to rapid fluctuations relative to the primary shear layer flame structure.

From this image set the CH* emission is found to be greater closer to the point of fuel injection at ER=0.6 and ER=1.0 than ER=0.8 and ER=1.1. In other words, the flame front is stabilized closer to the injection point and the flame is better anchored. Injection velocity increases as ER goes from 0.6 to 0.8 but is reduced again at ER=1.0 as a result of the nozzle change discussed previously. Under conditions of a higher fuel inlet velocity the low flame reaction zone is more likely to lift because increased fuel velocity. With a higher fuel velocity the fuel does not fully vaporize until it is farther downstream. This phenomenon is also observed within the OH* images [13]. This demonstrates the high sensitivity of the low flame structure to fuel pressure.

As ER increases CH* intensity in the mid-flame region is seen to increase while the CH* intensity near the flame base is seen to decrease. This indicates that, while more heat release occurs as a result of increased fuel flow rate, the region of high concentration tends to move from the low- to mid-flame region and the high-intensity region in the middle becomes more dominant. This is explained by two contributing factors. First, increased fuel flow rate requires more time to vaporize than a lower fuel flow rate. Second, at a higher global equivalence ratio the mixture near the fuel injection point will be richer and more time is required to achieve the mixing required for bulk combustion.

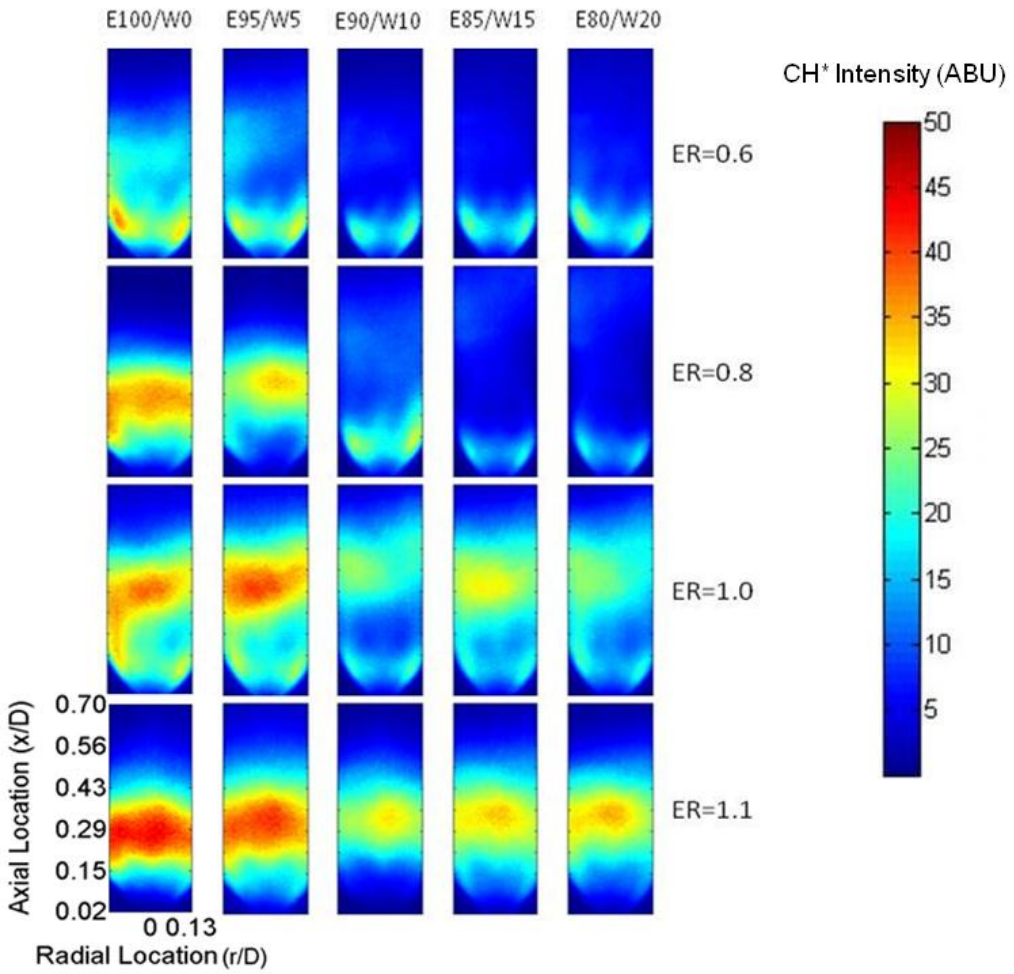

Figure 8: Time-Averaged, Run-Averaged CH* Images

Considering spatially averaged intensity of these figures with regards to changes in fuel composition reveals that CH* intensity in the field of view decreases as water content increases, regardless of equivalence ratio. Because of the limited field of view this reduction does not necessarily indicate reduced heat release over the entire combustor and may suggest the importance of ongoing combustion in other regions of the combustor, and that globally a more even distribution of heat release is experienced. These claims are later validated through exhaust gas composition analysis which reveals that the fuel is completely burned at the combustor exit for all cases considered. This implies that the addition of water relocates the bulk of combustion to regions not within the CH* viewing window. This is also indicative of near-field quenching of the reactions caused by the presence of water.

3.4 Axial Distribution of Time-Averaged CH* and OH*

The axial distribution of CH* and OH* was determined by first considering time-averaged run-averaged images. Then each row of pixels was averaged to give a single value. The resulting mean value for each pixel row was then plotted as a function of axial location. This process was completed for CH* and OH* at various equivalence ratios and fuel compositions. The results are displayed in Figure 9.

Considering ER=0.6 we see that both CH* and OH* exhibit a high intensity region between approximately x/D=0.110 and x/D=0.183 above the dump plane. A second peak in intensity occurs from approximately x/D=0.330 to x/D=0.513 above the dump plane. The first peak builds from the dump plane and indicates a region in which fuel is being vaporized before peak combustion is reached. There is

then a decrease in intensity before the second peak. This two peak structure is the result of the two high CH* regions observed previously in the CH* images. The first peak represents the primary, tulip-shaped, structure that is stabilized by the central recirculation zone. This structure fits within the field of view. The second peak indicates the presence of the secondary reaction zone much wider than the field of view of the windows. The separation between the peaks is less defined in the OH* images which is expected since OH* represents CH* oxidation and we can expect more uniform spatial distribution of OH* emission compared to the spatial distribution of CH*. At ER=0.6 it is evident that as water content increases heat release in the field of view decreases without substantially affecting flame structure.

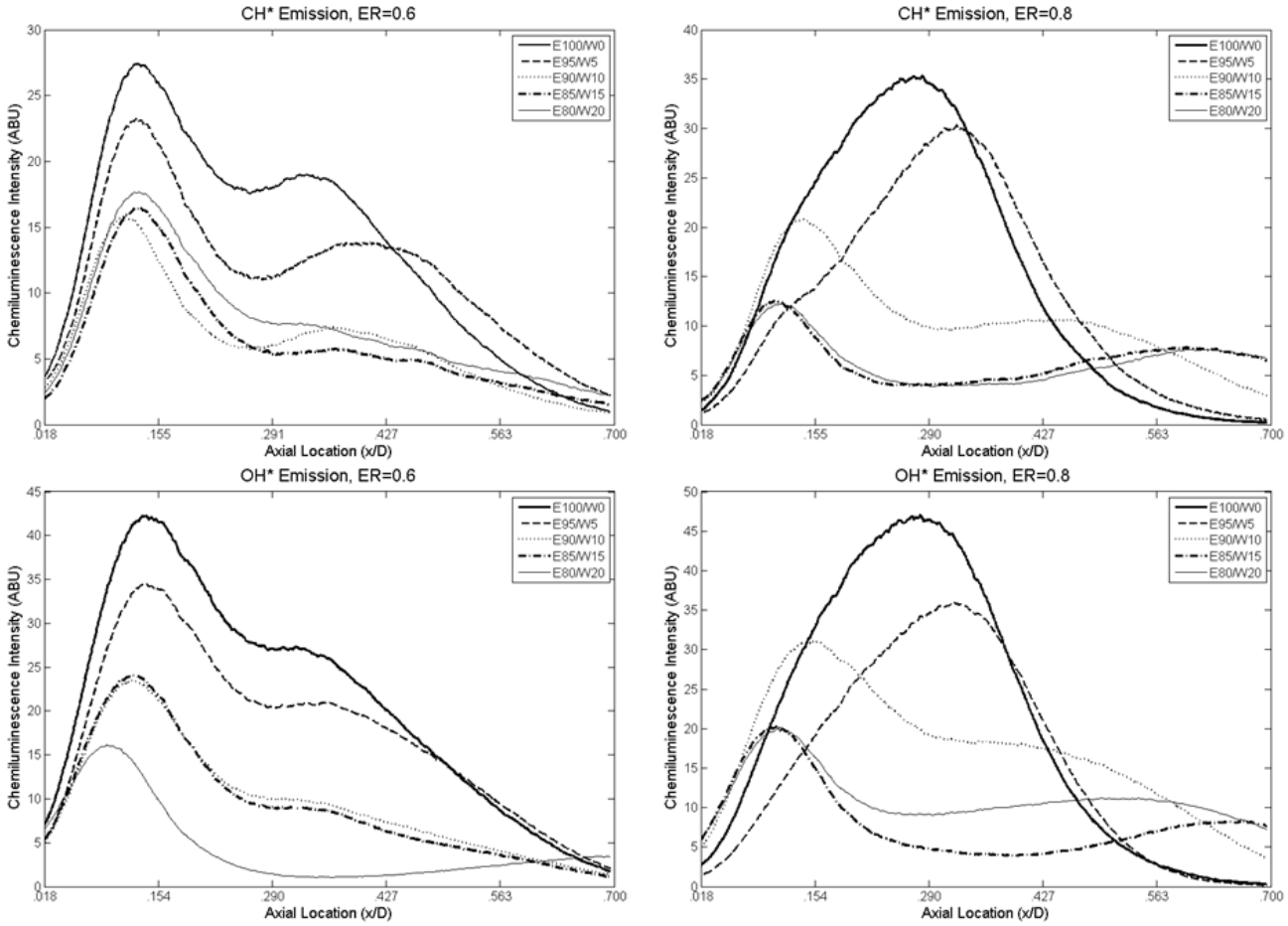

Figure 9: Axial Distribution of CH* and OH* Emission Within the Low-Flame Region

When equivalence ratio is increased to 0.8, for E100/W0 and E95/W5, a single large heat release peak is observed instead of the two smaller peaks previously described. This is consistent with the contour maps seen in Figure 8 where spray vaporization is pushed downstream because of higher momentum. For the higher water content fuels, significantly lower and flatter distributions are seen with CH* values remaining significant beyond the viewing window. This indicates that the presence of water has a quenching effect in the near-field, and combustion of the vaporized fuel continues downstream. This is also evident when considering the CH* intensity at the end of the viewing window (x/D=0.7) where CH* levels are generally seen to increase as water content increases.

This suggests that heat release from hydrous fuels continues outside the field of view and is spatially delayed. This observation is consistent with the temperature plots in Figures 4-7 where only small differences in temperatures are seen later in the combustor. This redistributed heat release leads to the lack of significant difference between exhaust gas temperatures.

3.5 Flame Tip CH* Imaging

Earlier CH* images presented in Figure 8 were taken through the lower viewing window. Since the combustion behavior extended beyond the lower window's field of view ($0.018 \leq x/D \leq 0.700$) line of sight CH* images were taken over a 12.7 x 7.62 cm region located 0.46-0.58 meters downstream of the dump plane ($1.67 \leq x/D \leq 2.13$). The CH* intensity in this region was lower and different gain settings were used compared to the lower window results. Images were taken at ER=1.0 for fuels ranging from E100/W0 to E80/W20. Three time-averaged images were combined to obtain a run-averaged time-averaged representation of CH* release in this region. These images were then spatially averaged to a single value which is presented in Figure 10. This data reveals that CH* intensity in this region is generally reduced as water content increases. This suggests that the flame is not appreciably lengthened as a result of water addition and that heat release near the flame tip is indeed reduced in the presence of excess water. From this plot it is apparent that CH* release at the flame tip is not solely dependent upon water content which suggests that flame length is appreciably affected by the inevitable changes in fuel spray velocity and atomization quality that result from increased volumetric fuel flow rate. Repeatability error bars are shown for reference.

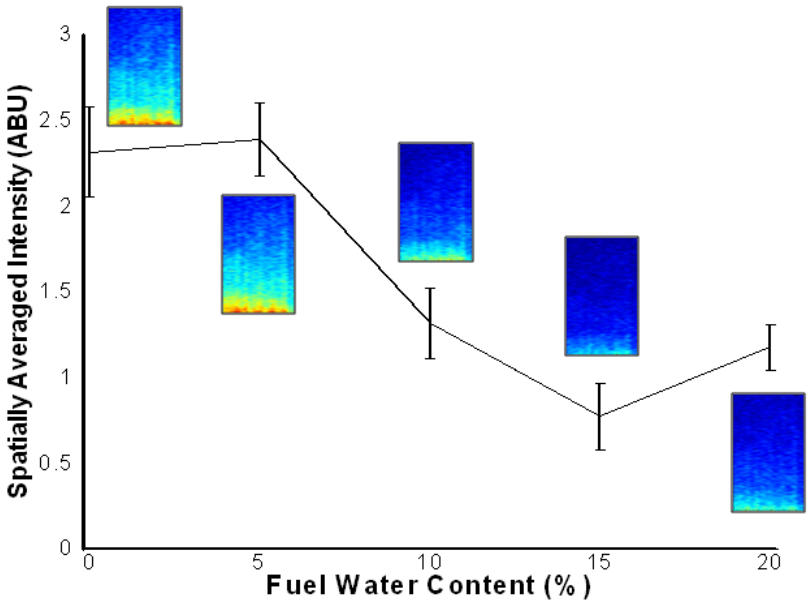

Figure 10: Flame Tip CH* Emission at ER=1.0

3.6 Exhaust Gas Temperature

Exhaust gas temperature was taken at two radial locations (5.71 and 8.85 cm from the centerline) at the combustor exit 0.84 meters downstream of the dump plane. These temperatures were averaged to evaluate the average temperature of the exhaust gas flow. This data was collected at least three times for each test condition. The results are shown in Figure 11. Repeatability error bars are displayed and indicate a reasonable level of repeatability.

This data shows a clear trend between exhaust temperature and equivalence ratio. As equivalence ratio increases the average exhaust temperature is seen to increase. This is predictable and is consistent regardless of fuel composition.

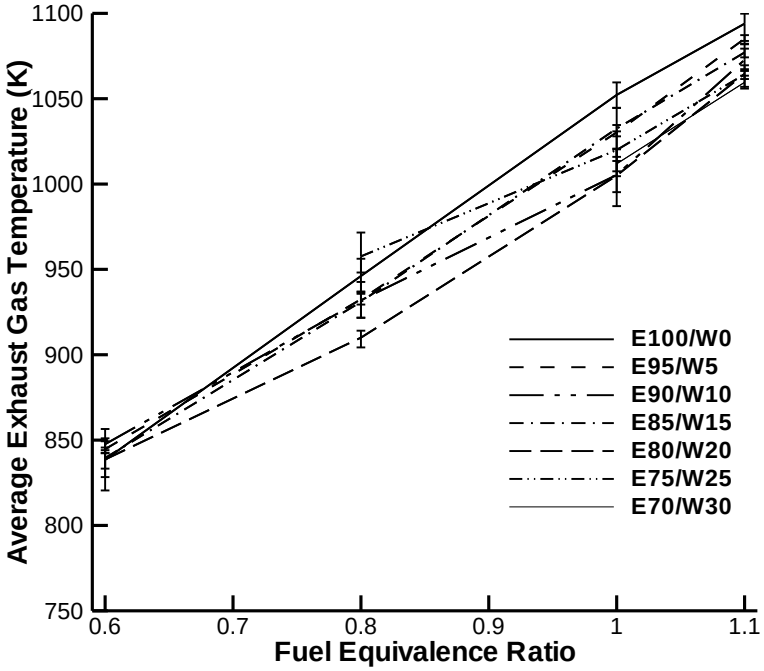

Figure 11: Average Exhaust Gas Temperature as a Function of ER and Fuel Composition

From this figure a 1:1 relationship between water content and average exhaust gas temperature is not clear. However, statistical analysis of the data reveals a Pearson's Correlation Coefficient (PCC) of -0.12 between exhaust temperature and fuel water content. This suggests that there is a weak correlation between the two parameters but that increasing water content leads to slight decreases in exhaust temperature. This makes sense because, for a particular ER, an increase in water content results in more heat absorption by water. Since more heat is devoted to phase change of water less heat remains for increasing exhaust gas temperature. However, since the correlation between the two parameters is weak it is relevant to note that there is an observable amount of variability that does not appear to depend on fuel composition. This variation is attributed to changes in fuel pressure and consequently spray characteristics that results from changing the volumetric flow rate as water content changes.

3.7 Exhaust NO_x Concentration

Exhaust gas was sampled from the combustor centerline at the combustor exit. NO_x concentrations within the gas were determined by the Cambustion NO_x Analyzer. This data revealed that NO_x is generally reduced as water content increases, regardless of equivalence ratio. There is no nitrogen in the fuel so all NO_x that is formed is either thermal NO_x or prompt NO_x. At no point did the exhaust NO_x concentration exceed 15 parts per million (PPM). Accuracy of exhaust NOx measurements is estimated to be less than +/- 1%.

At ER=0.6 it is found that the addition of 5% water to the fuel leads to a 33% reduction of exhaust NO_x. Additional increases in water content continued to lower the concentration of exhaust NO_x. A 15% water mixture was the most hydrous fuel that could be burned at ER=0.6 and resulted in a 49% reduction in exhaust NO_x when compared to pure ethanol. At ER=0.8 exhaust NO_x is seen to be reduced by 12%, 29%, and 40% for fuels containing 5%, 10% and 15% water respectively. When using a water content of 20% or 25% it was possible to achieve NO_x reductions of greater than 69%. However, the flow condition at these test points required the use of a different atomizing nozzle and therefore cannot be directly compared. At higher equivalence ratios it is seen that, with enough water addition, it is possible to keep exhaust NO_x concentration below 5 ppm even for ER=1.1.

By plotting exhaust NO_x concentration as a function of exhaust gas temperature instead of ER (the relationship between ER and exhaust gas temperature was studied previously) we find that exhaust temperature plays a significant role in predicting NO_x concentration. Please note that each discrete test condition was determined by targeting the range equivalence ratios described previously. Exhaust gas temperature and exhaust NO_x are both dependent variables that are controlled by ER. However, these two measurables are fundamentally linked and plotting in this manner reveals more basic conclusions. Considering the influence of exhaust gas temperature does not eliminate the dependence of exhaust NO_x concentration on fuel composition. Figure 12 displays this dependence and solidifies claims that increasing water content reduces NO_x. Repeatability error bars are shown and demonstrate reasonable repeatability for the data. Elevated water content leads to redistribution of heat and temperature which results in reduced peak temperatures within the combustor. Since peak temperatures are lower with higher water content, thermal NO_x formation is reduced.

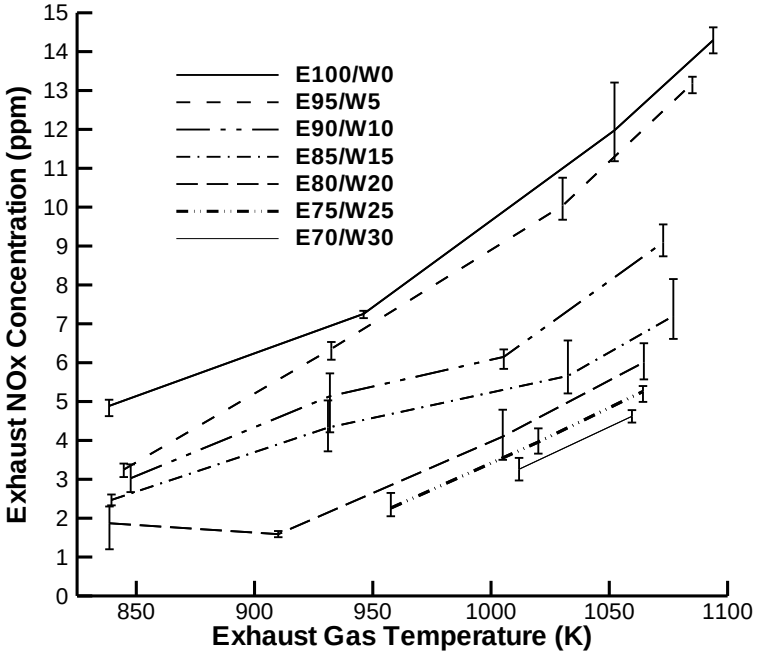

Figure 12: Exhaust Gas NOx Concentration as a Function of Exhaust Temperature and Fuel Composition

3.8 Exhaust O_2 Concentration

Exhaust gas sampled from the centerline at the combustor exit was analyzed using the Gas Chromatograph (GC). The GC is capable of resolving O_2 and CO_2 concentrations with an accuracy of +/-0.5%. Figure 13 shows the exhaust oxygen concentration presented as a function of water content. Considering the exhaust oxygen concentration as a function of equivalence ratio it is found that the mol fraction of oxygen in the exhaust generally decreases as fuel to air ratio increases. This is because adding more fuel to a lean mixture results in more combustion reactions and the consumption of more oxygen. All of the oxygen present in the exhaust gas is either excess oxygen or is oxygen that was not effectively mixed with unburned hydrocarbons. As the ER approaches unity the amount of excess oxygen decreases toward zero. This trend was observed for all fuel compositions regardless of water content. A slight increase in O_2 concentration is seen when ER increases from 1.0 to 1.1. This is caused by localized flame quenching that can occur as the mixture becomes rich.

Figure 13 shows that while some fluctuations in exhaust oxygen concentration are observed with different fuels the trend is generally flat between water content and the presence of oxygen in the exhaust.

This leads to the conclusion that combustion efficiency over the entire length of the combustor is not changed as a result of water addition.

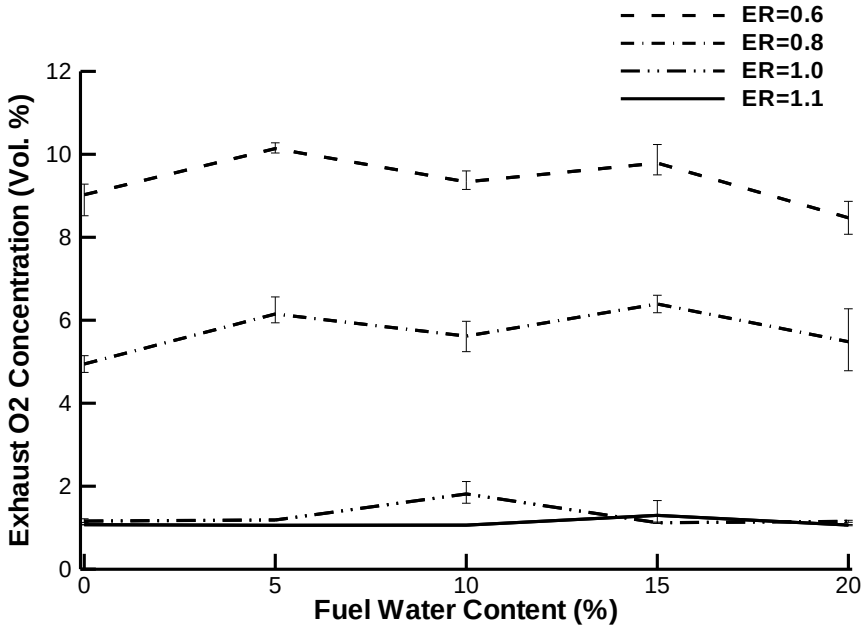

Figure 13: Exhaust Gas O_2 Concentration as a Function of Equivalence Ratio and Fuel Composition

3.9 Exhaust CO_2 Concentration

Considering the concentration of carbon dioxide in the exhaust gas we find trends that support the conclusions determined by observing exhaust O_2. As equivalence ratio increases towards unity the concentration of carbon dioxide in the exhaust is found to increase (Figure 14). This is because increasing fuel flow rate in a lean combustion reaction results in more complete combustion events because excess oxygen is present and the formation of the stable CO_2 product is encouraged by the presence of more C_2H_5OH. As equivalence ratio increases beyond unity the concentration of CO_2 in the exhaust is generally found to slightly decrease. This is because a rich combustion reaction will be starved of oxygen and will inhibit the formation of fully oxidized carbon. The reduction in CO_2 should be coupled with an increase of unburned hydrocarbons as well as an increase in incomplete combustion products such as CO or CH_4. These species were found at equivalence ratios greater than 1.0 and were found in greater concentrations at ER=1.1. Unfortunately the concentrations of these species were near the detection limit of the GC so quantitative data could not be presented. However, the presence of these species adds validity to the conclusions presented here. These trends were consistent for fuels of all compositions.

Figure 14 shows the exhaust CO_2 data presented with water content on the x-axis. This plot shows that there is no strong correlation or trend between exhaust CO_2 concentration and fuel water content. This plot reinforces the conclusions made previously that water content does not affect combustion efficiency over the combustor volume. Once again any variations between tests with different fuels can be attributed to changes in fuel pressure and spray characteristics. Repeatability is again excellent.

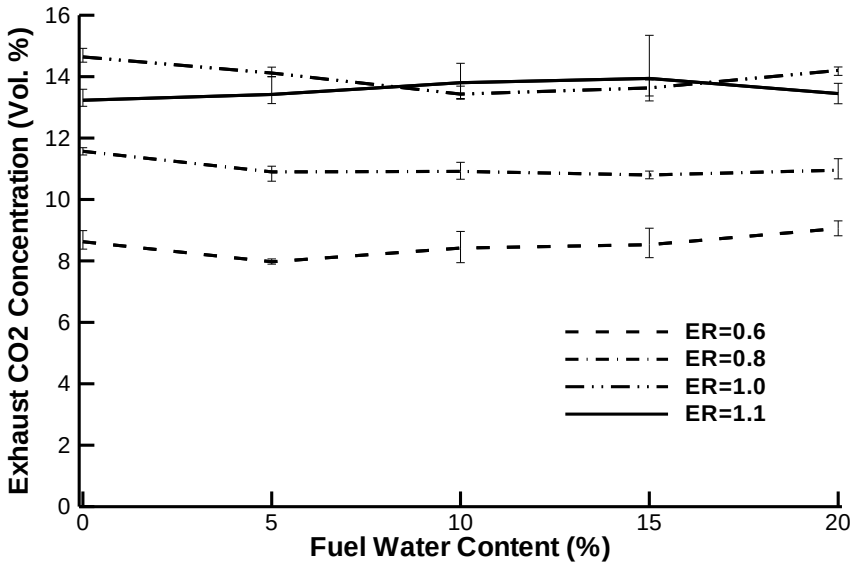

Figure 14: Exhaust Gas CO_2 Concentration as a Function of Equivalence Ratio and Fuel Composition

3.10 System Performance

It has been established that elevated water content generally leads to temperature reductions, both within the flame and in the exhaust, but exhaust gas concentration suggests that elevated water does not lead to reductions in combustion efficiency. At the same equivalence ratio and operating at the same combustion efficiency a hydrous fuel flame and an anhydrous fuel flame will release the same amount of heat over the entire combustor volume. However, at a given equivalence ratio hydrous fuels require more heat to vaporize. The presence of water provides a parasitic heat load on the flame. When heat is released it is devoted to water vaporization before temperature increase. Furthermore, increased mass flow rate of the fuel means more heat must be supplied to achieve the same temperature. At first glance it is expected that reduced exhaust temperature corresponds to decreased available heat in the exhaust gas stream and poor combustor performance. An analysis of heat flux into and out of the combustor leads to a different conclusion.

The rate of heat coming from the combustor exhaust is dependent upon the temperature of the exhaust, the mass flow rate through the combustor, and the average specific heat of the exhaust gas ($\dot{Q} = \dot{m}C_pT$). Exhaust heat rate was calculated for each fuel composition and equivalence ratio. The mass-weighted specific heat of the exhaust gas was calculated based on exhaust gas composition. Exhaust temperature was a measured value presented previously, and mass flow rate was calculated based upon fuel and air flow-rates. The results, shown in Figure 15, show that heat rate out of the combustor is not negatively affected by the addition of water. Pearson's Correlation Coefficient of 0.07 suggested a negligible correlation between fuel water content and exhaust heat rate. Reduced exhaust temperatures were off-set by the increase in mass flow rate required when burning hydrous fuel. This reinforces GC measurements suggesting that heat release over the entire combustor is not appreciably affected by the use of hydrous fuel.

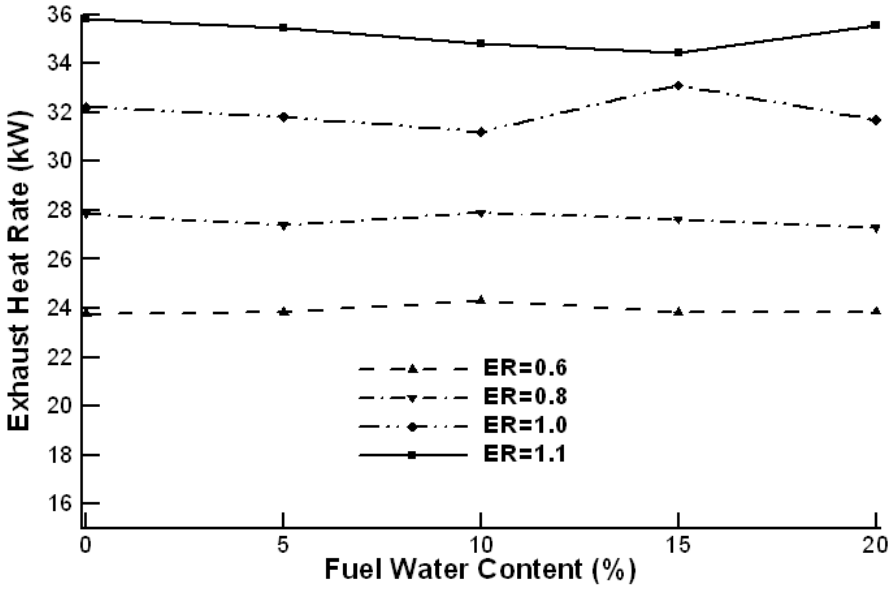

Figure 15: Exhaust Heat Rate as a Function of Equivalence Ratio and Fuel Composition

Calculations also revealed that the thermal efficiency of the combustor ($Eff = \frac{Exhaust\ Heat\ Rate}{Fuel\ Heat\ Potential}$) was not reduced as a result of water addition and actually improved slightly as water content increased. Thermal efficiency across the combustor was highest at ER=0.6 and lowest at ER=1.1. A leaner mixture leads to more complete combustion because of excess air and more complete mixing. Peak efficiency values of 57% were achieved. This number is reasonable for a non-adiabatic combustor that was not tuned specifically for maximum thermal efficiency. Considering the energy cost associated with distillation [9] it can be concluded that a life-cycle energy savings can be had if E85/W15 were used instead of E100/W0.

4. Conclusions

A study was performed to evaluate the feasibility of hydrous ethanol as a suitable fuel. Experimental evaluation of the fuel was performed and fundamental relationships between water content and flame temperature, exhaust NO_x, LBO, flame structure, exhaust gas composition, and chemiluminescence properties were observed. The following conclusions were made:

- A stable flame was achieved for fuels of up to E65/W35.
- The flame is not appreciably lengthened by the use of up to E80/W0.
- Despite reduced exhaust temperature, exhaust heat rate is not reduced by E80/W20.
- Combustion and thermal efficiency are not reduced by the use of E80/W20.
- Life-cycle energy savings of up to 25% can be had through the use of E85/W15.

In conclusion, this study has validated up to 20% water in ethanol as a practical fuel for continuous flame applications. This fuel can be produced at a lower capital cost than anhydrous ethanol and will provide an economic benefit despite increased volumetric consumption. The use of up to E80/W20 offers a reduction in exhaust NO_x concentration and a reduction in peak flame temperatures without reducing combustion efficiency or exhaust heat rate. Negative effects on flame stability are minimal and are restricted to extremely lean equivalence ratios. Despite the many advantages that can be had by using E80/W20, or any lesser water content fuel, the engine designer should be prepared to re-tune

fuel injection specifically for hydrous fuel since increased fuel flow rate will result in changes to the fuel spray characteristics and have significant implications on combustor performance.

Acknowledgements

This work was supported by a grant from the U.S Department of Energy through the Clean Power and Energy Research Consortium (CPERC). This support is gratefully acknowledged

Special thanks to Srinibas Karmakar and Shengrong Zhu for their assistance in developing instrumentation and experimental methods. Thanks also go to Chris Atenio and Ryan Keller for their handi-craft in apparatus development and maintenance.

References

[1] Heywood JB. Internal combustion engine fundamentals. 2nd ed. McGraw-Hill, 1998.

[2] Mack JH, Aceves SM, Dibble RW. Demonstrating direct use of wet ethanol in a homogeneous charge compression ignition engine, J. of Energy 2009; Vol. 34 Issue 6: p.782-7.

[3] Brewster S, Railton D, Maisey M, Frew R, The effect of E100 water content on high load performance of a spray guide direct injection boosted engine. SAE 2007-01-2648.

[4] Lefebvre AH, Ballal DR, Gas turbine combustion: alternative fuels and emissions. 3rd ed. Taylor and Francis Group, 2010.

[5] Bayraktar H. Experimental and theoretical investigation of using gasoline-ethanol blends in spark-ignition engines, J. of Renewable Energy 2011; Vol. 30 Issue 11: p 1733-47.

[6] Karmakar S, Dooley K, Acharya S. Combustion of boron nano-particles in ethanol spray flame. Proceedings, ASME IMECE 2010-37450.

[7] Wen D. Nanofuel as a potential secondary energy carrier. J of Energy and Environ. Sci, 2010; p. 591-607.

[8] Ladisch MR, Dyck K. Dehydration of ethanol: new approach gives positive energy balance, Science 1979; Volume 205, No. 4409, p. 898-900.

[9] Martinez-Frias J, Aceves S, Flowers D. Improving ethanol life cycle energy efficiency by direct utilization of wet ethanol in HCCI engines. J. of Energy Resources Technology 2007; Volume 129, p. 332-7.

[10] Cordon D, Clarke E, Beyerlein S, Steciak J, Cherry M. Catalytic igniter to support combustion of ethanol- water/air mixtures in internal combustion engines, SAE 2002-01-2863.

[11] Parag S, Raghavan V. Experimental investigation of burning rates of pure ethanol and ethanol blended fuels. Combustion and Flame 2009; Vol. 156, Issue 5: p. 997-1005.

[12] Gordon S, McBride MJ. Computer program for calculation of complex chemical equilibrium compositions and applications. NASA Reference Publication 1311, 1996.

[13] Breaux B, Karmakar S, Zhu S, Acharya S. Evaluation of hydrous ethanol combustion in a swirl stabilized combustor. ASME IMECE 2011-63688.

[14] Breaux B, Acharya S. The effect of elevated water content on ethanol combustion: a feasibility study. ASME POWER 2011-55301.

[15] Han D, Mungal MG. Simultaneous measurements of velocity and CH distributions, part 1: jet flames in co-flow. Combustion and Flame 2003; 132: p. 565–90.

[16] Najm HN, Paul PH, Mueller CJ, Wyckoff PS. On the adequacy of certain experimental observables as measurements of flame burning rate. Combustion and Flame 1998; 113: p. 312-32.

[17] Haber LC, Vandsburger U, Saunders WR, Khanna VK. An experimental examination of the relationship between chemiluminescent light emissions and heat-release rate under non-adiabatic conditions. RTO AVT Symposium, 2000.

[18] Barreta L, Jose da Rocha C, Carinhana D, Sbampato M, de Oliveira A, Monteiro dos Santos A. Emission spectroscopy of CH radical to determine the temperature of ethanol flame. Annals of Optics 2003; Volume 5.

[19] Zhu S, Acharya S. An experimental study of lean blowout with hydrogen enriched fuels in a swirl stabilized premixed combustor. ASME GT 2011-46096.

[20] Glassman I. Combustion. 3rd Ed. Academic Press. San Diego. 1996.